Monte Carlo simulations of polydisperse ferrofluids: Cluster formation and field-dependent microstructure

Tobias Kruse,[1] Anna Spanoudaki,[2,1] and Rolf Pelster[1]
[1]*II. Physikalisches Institut der Universität zu Köln, Zülpicher Strasse 77, 50937 Köln, Germany*
[2]*Laboratoire de Physique, Ecole Normale Supérieure de Lyon, 46, allée d' Italie, 69364 Lyon Cedex 07, France*
(Received 8 April 2003; published 26 August 2003)

We report on a Monte Carlo investigation of the microstructure of ferrofluids. The simulation parameters were chosen so that they reflect as close as possible the real ferrofluid samples that have been characterized experimentally. The consistency of the resulting equilibrium configurations with small-angle scattering data on the original samples allows us to consider the simulation a good description of the actual microstructure. We observe agglomerates consisting mainly of a small number of particles. The agglomeration probability is higher the larger the particle radius is. But also small particles (radius smaller than 5 nm) take part in the cluster formation. On applying an external magnetic field the agglomerates become elongated due to a rearrangement of the particles and orient themselves parallel to the field lines. We present a statistical evaluation of agglomeration degree, cluster sizes, and cluster composition (sizes of clustered particles) as well as of the field-dependent change of microstructure (orientation and shape anisometry of clusters).

DOI: 10.1103/PhysRevB.68.054208 PACS number(s): 61.46.+w, 77.84.Lf, 61.20.Ja, 75.50.Mm

I. INTRODUCTION

Ferrofluids are colloidal dispersions of magnetic monodomain nanoparticles in a carrier liquid.[1,2] In order to avoid permanent agglomeration, the particles are charged (ionic ferrofluids) or coated with a surfactant layer (surfacted ferrofluids). Nevertheless, attractive dipole-dipole and van der Waals interactions may lead to the formation of clusters. In a magnetic field, ferrofluids develop anisotropic macroscopic properties, including dielectric permittivity (magnetodielectric effect[3,4]), refractive index (magneto-optic effect[5–7]), and viscosity.[8–11] Evidently, this must be due to a field-induced anisotropic microstructure, i.e., due to the presence of nonspherical units (particles or clusters) having an orientation parallel to the applied field. Thus, ferrofluids are a rare example of composite material, the microstructure of which can be altered in a continuous and reversible way via an external parameter (magnetic field), while components and mixture ratio remain unchanged. They are, therefore, of special interest for the study of the correlation between microstructure and macroscopic properties of heterogeneous materials.

The simulation of magnetic or, in general, dipolar fluids using Monte Carlo (MC) methods has been employed for already more than 20 years in order to extract information on structure formation in such systems. Because of the limited computer capacities, the early investigations were performed on two-dimensional models.[12–15] Later, simulations were extended to three dimensions: most authors consider monodisperse and purely dipolar systems, i.e., equally sized particles with a repulsive core (soft or hard spheres) interacting solely via long-range dipole-dipole forces.[16–23] Even in the absence of an external magnetic field, aggregates (clusters) form. These are dynamic units in that, depending on the relation between the interaction potential and thermal energy, the particles can leave or join clusters. The microstructure depends on volume filling factor and dipolar coupling strength (so-called aggregation parameter or thermal coupling parameter)

$$\lambda = \frac{E_{\parallel}^{dd}}{2k_B T}, \tag{1}$$

where $E_{\parallel}^{dd}$ denotes the dipole-dipole energy of two clustered particles with parallel magnetic moments. For small $\lambda \geqslant 1$, i.e., in the so-called gas or vapor phase, some clusters consisting of a few particles can form (dimers, trimers, etc.). With increasing λ, i.e., with decreasing temperature or increasing particle size, the microstructure changes. There are two possible scenarios: the particles may align themselves in a nose-to-tail fashion, forming long chainlike structures.[16–22] The other possibility, which was only recently observed in MC simulations of purely dipolar systems, is the loss of aggregative stability resulting in decomposition into so-called ''gaslike'' and isotropic ''liquidlike'' phases (formation of experimentally observable droplike aggregates) (Ref. 23). For volume filling factors in the range $f = 1-10\%$, for example, this transition occurs near $\lambda = 3$ (see Fig. 8 in Ref. 23). According to the theoretical model of Ref. 24 the competition between isotropic and anisotropic interactions determines the microstructure at high λ: the orientationally averaged potential energy, $\langle E \rangle$, drives condensation in droplike aggregates, while anisotropic dipolar interactions, i.e., the deviation $E - \langle E \rangle$, are responsible for chain formation. In fact, simulations show that additional isotropic attractive short-range interactions, such as van der Waals, favor liquid-vapor coexistence (modelization via a Lennard-Jones potential in Stockmeyer fluids[25,26]). This picture changes when a magnetic field is applied: the forces between oriented magnetic dipoles are highly directional, so that the energy of the system cannot be greatly reduced by condensation to a denser isotropic fluid phase.[27] Instead, clusters align along the field lines, i.e., depending on the microstructure either chains unfold and/or orient themselves or droplike aggregates become elongated[18,19,26] (experimental studies indicate

the existence of anisometric structures, such as bundlelike aggregates,[28] that orient themselves in an external field[28–31]).

Although the aforementioned simulations and models give a quite consistent picture of the dynamics in monodisperse fluids, they are not directly applicable to real ferrofluids, since these do not consist of equally sized spheres. The magnetic moment of a particle depends on its radius, $\mu_i \propto R_i^3$, so that polydispersity in size implies altered interactions and thus has a direct effect on microstructure. For example, both experimental[34] and theoretical[35] studies indicate that polydispersity finds expression in phase diagrams of ferrofluids. Simulations of a hard-sphere fluid with a Gaussian distribution of particle sizes and thus dipole moments have been carried out in the limit of strong and purely dipolar interactions (average aggregation parameter $\langle\lambda\rangle_{avg}=6.25$, $f=40\%$) (Ref. 36). They showed that polydispersity significantly reduces the spontaneous orientational order observed in the ferroelectric phase of monodisperse models at high densities and low temperatures. To our knowledge there are no detailed simulations in the range where real ferrofluids find their applications, i.e., at much lower concentrations and at temperatures where the carrier liquid is not yet solidified, so that $\langle\lambda\rangle_{avg}\leqslant 1$ (in Ref. 37 simulated equilibrium configurations for systems at room temperature are shown, but the effect of polydispersity on the microstructure is not discussed). Especially, the question arises, to what extent particles of different sizes (radii R_i) take part in cluster formation. This becomes clear when we rewrite the aggregation parameter of Eq. (1) as[31]

$$\lambda=\left(\frac{R_1}{R_{limit}}\frac{R_2}{d_C}\right)^3. \tag{2}$$

Here d_C denotes the center-to-center distance of the clustered particles,

$$R_{limit}=\left(\frac{\mu_0 9 k_B T}{4\pi M_p^2}\right)^{1/3}, \tag{3}$$

and M_p is the saturation magnetization. A typical value for a real magnetite based ferrofluid at room temperature is $R_{limit}=2.8$ nm (see Ref. 31). Thermal stability of a cluster requires at least $\lambda\geqslant 1$, a condition that small particles with $R_1\leqslant\lambda^{1/3}\times R_{limit}$ can never fulfill, whatever the size R_2 of the second particle is. Nanoparticles with radius $R_1=4-5$ nm, a value that corresponds to the mean particle size in our ferrofluid samples (see below, Fig. 1), can only form pairs with $\lambda>1$ when combined with rather large particles that make up only a small portion of the size distribution (for details we refer to Ref. 31). Some theoretical models even favor a bidisperse approximation, where they distinguish between large particles forming aggregates and small particles that remain in the individual nonaggregated state.[9,32,33] Nevertheless, based on information on size distribution and interparticle distances gained from two-dimensional small angle x-ray scattering (2D-SAXS), we have shown that clusters in surfacted ferrofluids contain particles of all sizes: there is no division in smaller single and larger agglomerating particles (see also experiments on ionic ferrofluids in Ref. 34). We thus concluded that the short range but strong van der Waals forces must contribute significantly to the stability of the clusters. The effect of different particle sizes has also been studied theoretically applying the density function approach to a bidisperse model system (a majority of small particles, $R_1\simeq 4$ nm, and a small portion of large particles, $R_2\simeq 8$ nm).[38] This gives some indications of what might happen also in polydisperse systems, although only linear aggregates are considered: Under ''real conditions,'' i.e., at room temperature and for volume filling factors of 1–5%, the most typical topological cluster structure consists of short chains with 1–2 large particles in the middle and 1–2 small particles at the edges. All in all, a portion of 20–60% of small particles is aggregated. It is of practical relevance to obtain further information on the field-dependent geometry of clusters (number of particles, form, and orientation). Their size and shape distributions determine *inter alia* the rheological properties of magnetic fluids (see theoretical models in Refs. 8–11 and experiments in Refs. 33,39). Thus, polydispersity is of twofold importance: with regard to single particles it affects the formation of agglomerates, the nonuniformity of which, in turn, has an impact on macroscopic properties.

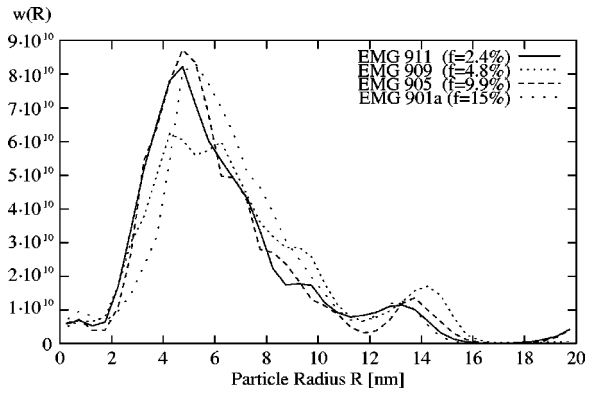

FIG. 1. Volume-weighted size distribution of magnetite particles in sample EMG 911, as determined through SAXS (Ref. 31).

Summarizing, it seems worthwhile to study in more detail the microstructure of polydisperse systems in the aforementioned range of concentration and interparticle forces. Especially, we are interested in size and form of the clusters and in how anisotropy develops in an external magnetic field. In order to represent correctly the microstructure of real ferrofluids, we take both long-range magnetic dipole-dipole and short-range van der Waals interactions into account. Moreover, we model specific ferrofluid samples, i.e., we set all relevant physical parameters with reference to existing ferrofluids: (i) the concentration, (ii) the particle-size distribution that reflects in the aforementioned interaction energies, (iii) the particle magnetization, and (iv) the thickness of the surfactant layer determining the closest approach distance between the particles and thus the role played by the short-range but strong van der Waals forces. All these parameter values that enter the Monte Carlo simulation were justified by appropriate measurements or by literature or manufacturer's data (Sec. II). This way we are able to control whether the resulting equilibrium configurations are consistent with

TABLE I. Saturation magnetization M_S, density ρ, and volume fraction f of magnetite for the experimentally characterized samples.

Ferrofluid Samples			
	$M_S(mT)$	$\rho(g/cm^3)$	$f(\%)$
Isopar	0	0.78	0.0
EMG 911	10	0.88	2.4
EMG 909	20	0.98	4.8
EMG 905	40	1.19	9.9
EMG 901a	60	1.42	15.0

experimental x-ray scattering data (Sec. V). Finally, we present a statistical evaluation of clusters in terms of size, composition, and field-induced elongation (Sec. VI). In a contribution to follow, we shall use these results to study the correlation between field-dependent microstructure and the macroscopically measured dielectric function in order to quantitatively explain the magnetodielectric effect.

II. SAMPLE SYSTEMS

In particular, we refer to surfacted ferrofluids consisting of Fe_3O_4 nanoparticles in Isopar-m. The samples were purchased from Ferrofluidics GmbH, Nürtingen, Germany and were of the nominal types EMG 901, 905, 909, and 911. In Table I the manufacturer's data for the saturation magnetization M_S and the results of density measurements for the volume fraction f in magnetite are shown. The table can be found in more detail and commented in Ref. 31. Using this data we calculate the mean particle magnetization $M_p = M_S/f = 0.4025$ T. Figure 1 shows the size distribution of the particles, which has been determined through SAXS.[31] The mean radius of the particles is $\overline{R} \simeq 4-5$ nm and the size distribution is rather broad, with a half width of 4–5 nm. The nanoparticles are covered with an oleic acid surfactant of chain length 2 nm. It stabilizes the colloid against permanent agglomeration, keeping the particles at distances at which their van der Waals potential is reduced to at most the order of magnitude of the thermal energy.

2D-SAXS measurements in an external magnetic field gave us information on cluster formation as well as on the asphericity of the particles.[31] Field-induced orientation of single particles is well described, treating them, on an average, as rotational ellipsoids with a small axis ratio $k_{eff} = 1.05$, that are fully oriented above a saturation induction of $B_s \simeq 0.3$ T. The above axis ratio is an average value that takes both the shape and the orientation into account, i.e., either the particles are almost spherical or, if this is not so, they do only partially orient along the field lines. The first possibility is supported by TEM investigations.[30] 2D-SAXS also revealed the presence of clusters in the colloid, in which the mean center-to-center distance of adjacent particles is about 10 nm. Accordingly, the mean radius of clustered particles is very close to the overall mean radius. The van der Waals interaction energy of such small particles can even exceed their magnetic dipole-dipole energy when they are separated by distances of the order of 1 nm.[31]

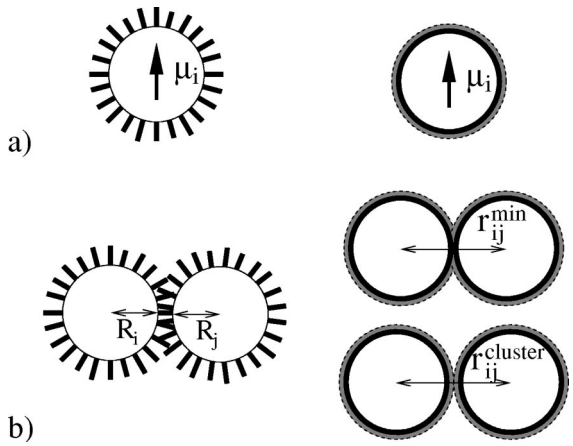

FIG. 2. (a) Left: sketch of a magnetite particle of radius R_i and magnetic moment μ_i, covered by a surfactant layer of oleic acid spacer molecules. Right: the surfactant layer of each particle is modeled as a double layer consisting of an inner hard shell of radius $1.1R_i$, covered by an outer soft shell of radius $1.2R_i$. The latter allows for a distribution of interparticle spacings in clusters. (b) Left: a cluster of two magnetite particles with partially interpenetrating surfactant layers. Right: the inner hard shell defines the minimum center to center distance r_{ij}^{min} between the particles [see Eq. (7)]. The outer soft shell defines the maximum distance $r_{ij}^{cluster}$ at which the particles still can be considered to form a cluster [see Eq. (6)].

III. GEOMETRY AND INTERACTIONS OF PARTICLES

In this section we define the model used to describe the geometry and interactions of the system to be simulated. We consider a polydisperse ensemble of magnetite particles (Fe_3O_4) covered with a surfactant layer of oleic acid spacer molecules [see Fig. 2(a)]. The magnetite core accounts for magnetic dipole-dipole and van der Waals interaction between particles, while the surfactant layer determines the steric interaction and defines a range of interparticle distances within clusters.

A. Magnetic core

As we mentioned in Sec. II, both SAXS (Ref. 31) (indirectly) and TEM (Ref. 30) studies (directly) show that the magnetite particles are in a good approximation of spherical shape. The small deviations observed should not affect considerably the interparticle interactions and thus the spatial distribution of particles. Therefore, the magnetic core can be simply represented as a hard sphere of radius R_i, carrying a magnetic dipole moment $|\boldsymbol{\mu}_i| = (4/3)\pi R_i^3 M_p$, where $M_p = 0.4025$ T denotes the mean particle saturation magnetization (see Sec. II). As mentioned in the Introduction, the degree of polydispersity may affect considerably the microstructure. In our simulations we therefore use ensembles of particles with a size distribution of log-normal shape fitting the actual size distributions of the samples (see Fig. 1 and Ref. 31). In order to obtain a good statistical representation

with a limited number of particles, we set $R_{max}=10$ nm. These bigger particles make up for about 10% of the volume. The above procedure also avoids artificial giant dipole moments that do not exist in real ferrofluids, since huge particles would not be magnetically monodomain.

The long-range dipole-dipole force governs the interparticle interactions at large particle distances. A particle i with magnetic moment $\boldsymbol{\mu}_i$ at position $\boldsymbol{r}_i$ will interact with the dipole field $\boldsymbol{B}_j(\boldsymbol{r}_i)$ produced by a second particle j at $\boldsymbol{r}_j$. At a center-to-center distance $r_{ij}=|\boldsymbol{r}_j-\boldsymbol{r}_i|$ the potential energy is

$$E_{ij}^{dd}(r_{ij}) = -\boldsymbol{\mu}_i \boldsymbol{B}_j(\boldsymbol{r}_i) = \frac{\mu_0}{4\pi}\left(\frac{\boldsymbol{\mu}_i\boldsymbol{\mu}_j}{r_{ij}^3}-3\frac{(\boldsymbol{\mu}_i\boldsymbol{r}_{ij})(\boldsymbol{\mu}_j\boldsymbol{r}_{ij})}{r_{ij}^5}\right). \tag{4}$$

At close surface approach the van der Waals (vdW) interaction can be of the same order of magnitude. The potential energy related to it,[40]

$$E_{ij}^{vdW}(r_{ij}) = -\frac{A_H}{6}\ln\left(\frac{r_{ij}^2-(R_i+R_j)^2}{r_{ij}^2-(R_i-R_j)^2}\right) - \frac{A_H}{6}\left[\frac{2R_iR_j}{r_{ij}^2-(R_i+R_j)^2}+\frac{2R_iR_j}{r_{ij}^2-(R_i-R_j)^2}\right], \tag{5}$$

is proportional to the Hamaker constant A_H. The estimation of this constant is quite complicated,[41] its value depending on the dielectric properties of particles, surfactant, and carrier liquid. For Fe_3O_4 particles in kerosine (Isopar-m) A_H is of the order of magnitude of 10^{-19} J within an uncertainty factor of three.[1,30] Using a convergence criterion we have fixed a value of $A_H=0.5\times10^{-19}$ J for our simulations (for details see below).

B. Surfactant layer

The inverted micelle structure of the surfactant layer leaves enough free volume for a partial interpenetration of adjacent layers in clusters,[42] as is schematically shown in Fig. 2(b) (left). In addition, the surfactant chains can be entangled or tilted. TEM studies on ferrofluids[30] have shown that the surface-to-surface distance of magnetite particles can be as small as 0.7 nm, at least after removal of the carrier liquid. Of course, the interparticle separation in a cluster can vary. The chain length of the spacer molecules yields an upper limit of 2×2 nm, although our 2D-SAXS studies revealed a much lower average separation.[31] In order to model the two main functions of the surfactant layer, i.e., defining a minimum distance between the particles as well as allowing for the formation of nonpermanent agglomerates in a certain range of distances, we chose a simple description as a two-shell model (see Fig. 2, right): two particles with magnetic core radii R_i, R_j are considered as clustered, as soon as they approach each other within a distance $r_{ij}^{cluster}$, which corresponds to contact of their surfactant shells (or the surfactant molecules' tails). In this way we record thermally stable as well as fluctuating clusters, which is important since both types contribute to the average microstructure determining macroscopic quantities such as the dielectric function. We define the radius of the surfactant shell for each molecule i equal to $1.2R_i$, so that the clustering criterion is

$$r_{ij}^{cluster}=1.2(R_i+R_j) \tag{6}$$

(note that such a static clustering criterion based on proximity of particles has also been used for monodisperse systems[17,20,43]). For the biggest particles in our simulation, $R_i=R_j=10$ nm, this yields a value of 24 nm corresponding to a surface-to-surface distance of 4 nm, i.e., twice the length of the spacer molecules. The shell thickness and consequently the interparticle spacing was chosen to be proportional to the radius of the magnetic core, reflecting the fact that smaller particles have a stronger surface curvature and thus a lower average surfactant density. This results in a higher free volume and should facilitate a better interpenetration of adjacent layers in a cluster.

The particles are allowed to approach each other to distances closer than $r_{ij}^{cluster}$, until they come to a distance r_{ij}^{min} at which the steric interaction does not allow a further interpenetration of the surfactant layers. In general, these steric interactions will depend on the exact distance $r_{ij}\in[r_{ij}^{min},r_{ij}^{cluster}]$ between two particles in contact. Nevertheless, for lack of a detailed microscopic theory we choose the most simple model, i.e., a potential energy

$$E_{ij}^{s}(r_{ij})=\begin{cases}\infty & \text{if} \quad r_{ij}<r_{ij}^{min}\\ 0 & \text{otherwise,}\end{cases}$$

defining the minimal center-to-center approach distance as

$$r_{ij}^{min}=1.1(R_i+R_j). \tag{7}$$

That is, regarding the steric repulsion the simulation procedure treats magnetic core and surfactant layer as a hard sphere of radius $1.1R_i$. With this choice, two particles of mean radius R=5 nm can approach to a minimal surface-to-surface distance of 1 nm, that is, comparable to that observed in TEM studies (about 0.7 nm, see Ref. 30). According to the above, depending on the tilt of spacer molecules and on the interpenetration of surfactant layers, particles can form clusters in a range of distances $[r_{ij}^{min},r_{ij}^{cluster}]=(R_i+R_j)[1.1,1.2]$.

C. Total potential energy of a particle

Summarizing, the particles in our simulations interact via magnetic dipole-dipole, van der Waals, and steric forces. If, in addition, we consider an external magnetic field (uniform magnetic induction $\boldsymbol{B}$), the total potential energy of each particle becomes

$$E_i^{tot}(\boldsymbol{r}_i,\boldsymbol{\mu}_i)=\sum_{j\neq i}\{E_{ij}^{s}+E_{ij}^{vdW}+E_{ij}^{dd}\}-\boldsymbol{\mu}_i\boldsymbol{B}. \tag{8}$$

The above interactions determine the spatial distribution of particles as well as the orientation of their magnetic moments.

IV. MONTE CARLO SIMULATION: ALGORITHM AND CONVERGENCE

A. Algorithm

At first, we define a cubic cell with side length L of 20–25 times the mean particle radius, corresponding to 100–150 nm. Depending on the concentration of the sample to be simulated, we distribute N particles in this volume ($N \simeq 140$–1300): we choose randomly position $\boldsymbol{r}_i$ and orientation $\boldsymbol{\mu}_i/|\boldsymbol{\mu}_i|$ of each hard sphere of radius $1.1R_i$, excluding any overlap. In order to minimize edge effects, we set periodic boundary conditions. Following the Metropolis algorithm[44] we assume a random translation and rotation of a given particle and calculate the corresponding change of potential energy, ΔE_i [see Eq. (8) and below]. If the Boltzmann factor $\exp(-\Delta E_i/kT)$ is greater than a random number $q_i \in [0,1]$, the attempt is accepted, otherwise the original particle coordinates are restored. The maximal translation length was chosen, so that the acceptance probability was 0.5.[45] A Monte Carlo step is a series of N attempts, so that on average each particle is chosen once. After a number of Monte Carlo steps thermal equilibrium is reached, i.e., the total energy of all particles does not change significantly any more and the simulation is stopped. The results we present in the following Secs. V and VI (Figs. 6–14) were gained after averaging over an adequate number of cells, so that the total number of particles simulated was about 3500, even at low filling factors. This guarantees a sufficiently good statistical representation of particle-size distribution and spatial configuration.

We have imposed periodic boundary conditions, but a numerical calculation of potential energies is only possible for a finite number of particles [see Eq. (8)]. Steric and van der Waals interactions are short range, so that it is sufficient to take only contributions from particles within a distance r_c into account. This range was chosen equal to seven times the particle radius. A further increase did not change the results (see also Ref. 46). On the other hand, long-range dipole-dipole interaction cannot be neglected for $r_{ij} \geqslant r_c$, but it would be too time consuming to sum up all contributions from particles at large distances [see Eq. (4)]. Therefore, we use the reaction-field method[47,48] that is faster than the often applied Ewald-Kornfeld summation technique.[45,49] For $r > r_c$ the sample is treated as a homogeneous medium. It is exposed to the magnetic field produced by the particles inside the sphere and it reacts with a magnetic induction $\boldsymbol{B}_R^i$, the so-called reaction-field. For a finite sample with demagnetizing factor 1/3 in an external induction $\boldsymbol{B}$, Eq. (8) becomes[47,48,50]

$$E_i^{tot} \simeq \sum_{\substack{j \neq i \\ r_{ij} < r_c}} \{E_{ij}^s + E_{ij}^{vdW} + E_{ij}^{dd}\} - \boldsymbol{\mu}_i(\boldsymbol{B}_R^i + \boldsymbol{B}) \tag{9}$$

with

$$\boldsymbol{B}_R^i = \frac{2(\mu_{eff}-1)}{2\mu_{eff}+1} \frac{\mu_0}{4\pi r_c^3} \sum_{\substack{j \\ r_{ij} < r_c}} \boldsymbol{\mu}_j . \tag{10}$$

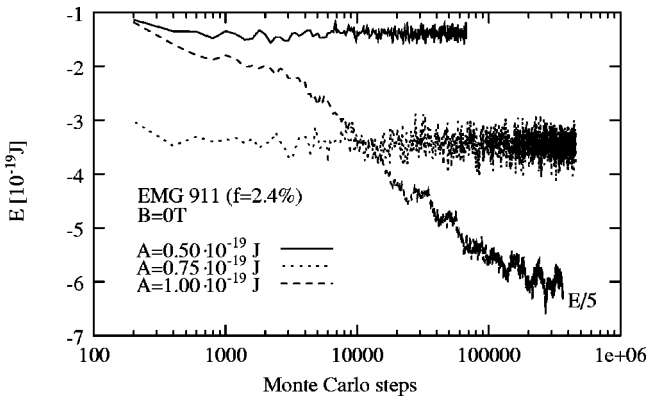

FIG. 3. Total potential energy as a function of Monte Carlo steps: the convergence depends on the strength of van der Waals interaction, i.e., on the choice of the Hamaker constant A_H [see Eq. (5)].

The effective permeability μ_{eff} depends on the total magnetization of the simulation cell of volume L^3, so that

$$\mu_{eff} = 1 + \frac{\mu_0}{B} \frac{\left| \sum_{k=1}^{N} \boldsymbol{\mu}_k \right|}{L^3} . \tag{11}$$

The sum of all dipole moments is calculated self-consistently in every Monte Carlo step, whereas at $B=0$ we use an extrapolated value.

B. Choice of Hamaker constant and convergence

The last open parameter for our simulations is the Hamaker constant A_H that determines the strength of van der Waals interaction [Eq. (5)]. As mentioned above, it is of the order of 10^{-19} J within an uncertainty factor of three.[1,30] Figure 3 shows the total potential energy of a simulated system of 500 particles as a function of Monte Carlo steps. For the two lower values $A_H = 0.5 \times 10^{-19}$ J and $A_H = 0.75 \times 10^{-19}$ J, the total energy converges to a stable value already after less than 10^4 steps, showing that the system has reached dynamic equilibrium. On the contrary, for $A_H = 1.0 \times 10^{-19}$ J, particle interactions are very intense and formation of agglomerates leads to a slow and continuous decrease of energy. Even after 4×10^5 steps no equilibrium is reached. Such an intense attractive van der Waals interaction would lead to complete agglomeration and phase separation (agglomerates/carrier liquid), which is not observed in ferrofluids of interest, including our samples. For our simulations we fix a value of $A_H = 0.5 \times 10^{-19}$ J, so that the most dense systems with 3500 particles reach thermal equilibrium after ca. 10^5 Monte Carlo steps. With this choice of A_H the van der Waals energy of two equally sized clustered particles at distance r_{ij}^{min} equals their total kinetic energy at room temperature, $2k_BT$ [see Eqs. (5) and (7)].

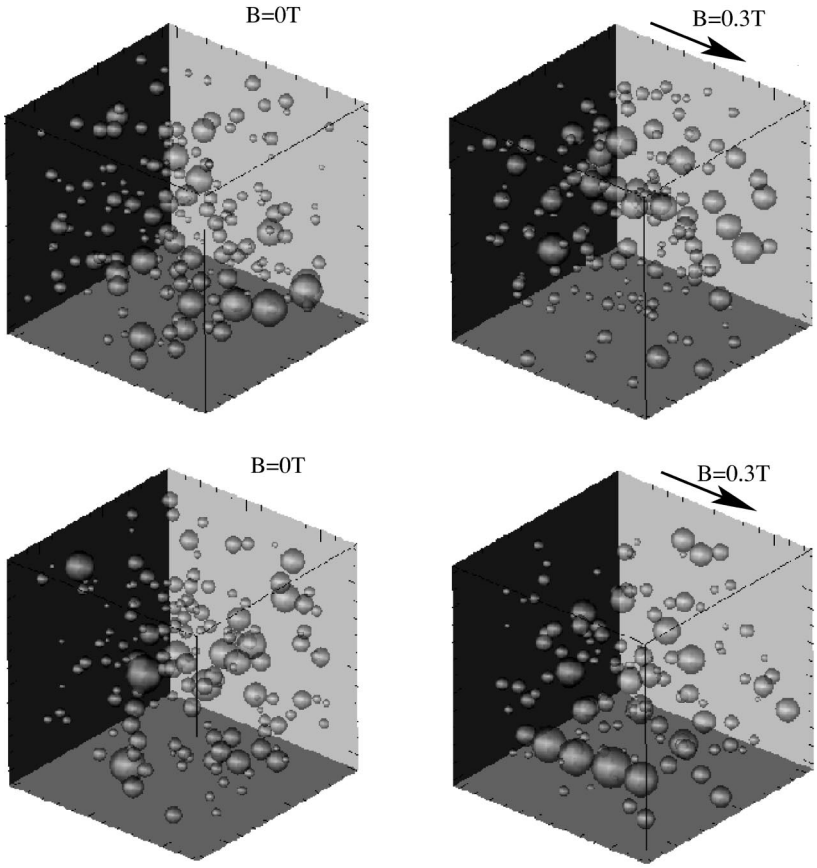

FIG. 4. Visualization of two simulated equilibrium configurations for sample EMG 911 ($f=2.4\%$). Left side: without external magnetic field. Right side: at saturation induction $B=0.3$ T. Note that particles crossing the wall of a simulation cell are also shown, so that the displayed volumes are slightly bigger than L^3.

V. CONSISTENCY OF SIMULATED MICROSTRUCTURE: A COMPARISON WITH EXPERIMENTAL 2D-SAXS DATA

In Figs. 4 and 5 we present Monte Carlo simulation snapshots based on systems with filling factor and particle-size distribution corresponding to those of samples EMG 911 and EMG 909 (volume filling factors $f=2.4\%$ and $f=4.8\%$, respectively). In zero field $B=0$ the spatial distribution of the particles appears to be isotropic. The particles group themselves, though, in small clusters consisting of a few particles. Most of the larger particles with high dipole moments are found to belong to clusters. Nevertheless, clusters also contain small particles (see also the theoretical model in Ref. 38). In an external magnetic induction of saturation, $B=B_s=0.3$ T, chainlike structures appear. These are similar to those found in other Monte Carlo simulations of polydisperse systems at room temperature.[37] The elongated agglomerates are oriented with their axis parallel to the field direction. This is how under the influence of a magnetic field the microstructure of ferrofluids becomes anisotropic, a fact that is reflected in their macroscopic properties as they are measured in SAXS, dielectric or rheological experiments. Before analyzing details of the resulting equilibrium configurations, such as size, composition, and shape of clusters (see below, Sec. VI), we have to control whether the spatial distribution of particles corresponds to that in real ferrofluids. As a reference we use experimental 2D-SAXS data[31] reflecting the microstructure of the samples listed in Table I. The simulation output (position, orientation, and volumes of the particles) gives us all the information we need to calculate the scattered intensity we would expect in a SAXS experiment. This data is then compared to the measured intensities.

In small-angle x-ray scattering on a system of N particles, the scattered intensity $I(\boldsymbol{h})$ as a function of the scattering vector $\boldsymbol{h}$ is described by

$$I(\boldsymbol{h}) \propto \left(\sum_i F_i^2(\boldsymbol{h}) + \sum_{i \neq j} F_i(\boldsymbol{h}) F_j(\boldsymbol{h}) \cos(\boldsymbol{h} r_{ij}) \right), \quad (12)$$

where $F_i(\boldsymbol{h}) = V_i \Phi_i(\boldsymbol{h})$ is the product of the particle volume V_i and its form factor.[51] Although the particles have been modeled as spheres in the Monte Carlo simulations, we have to correct for a small asphericity, due to the field-induced orientation of single particles at high B (see Ref. 31), which becomes noticeable in the measured intensity patterns at large h values. Thus we use the form factor of orientational ellipsoids[51] with small axis R_i and axis ratio k, whereas the orientation of the longest axis of each particle is assumed to coincide with that of its magnetic moment. We set $k=k_{eff}=1.05$, which is the effective axis ratio that we have previously determined by analyzing our experimental 2D-SAXS data at saturation induction $B_s=0.3$ T (see Sec. II and Ref. 31). At $B=0$ the above choice of k is of no importance, since single particles are randomly oriented. At $B \geqslant B_s$ it is only correct if the simulation yields an almost complete orientation of single particles. We now calculate the intensity according to Eq. (12) at scattering vectors $h_n = 2\pi(n/L)$ with $n \in N^*$. In doing so we avoid nonphysical oscillations

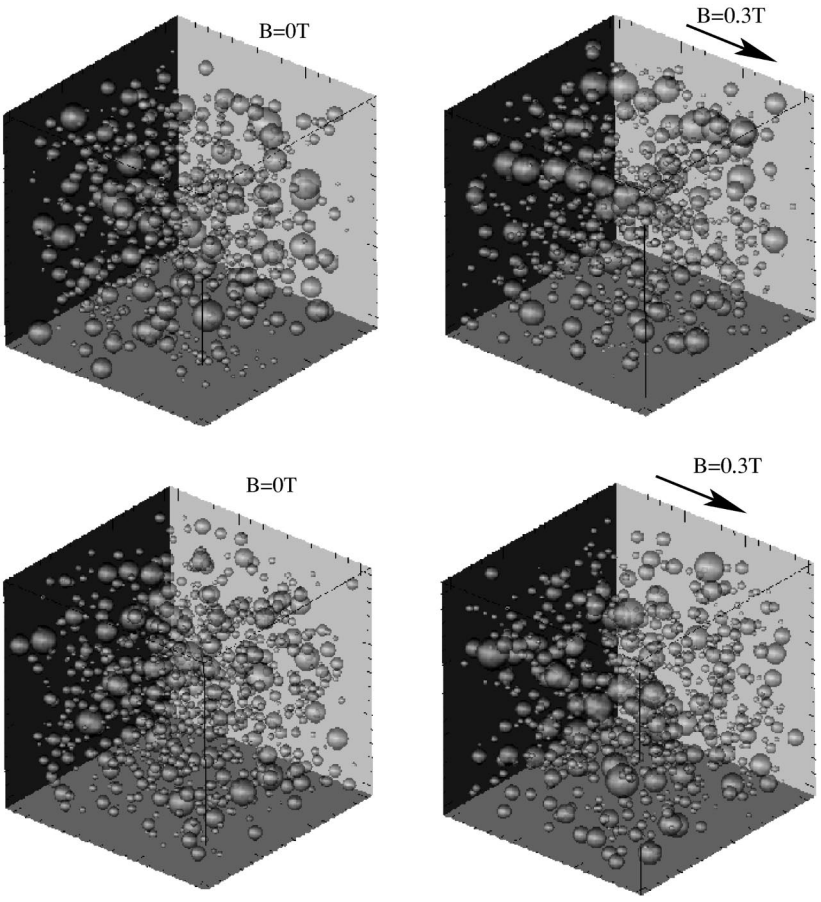

FIG. 5. Same as Fig. 4, for sample EMG 909 ($f=4.8\%$).

caused by the finite cubic simulation cell (volume scattering; for details see Ref. 52). As already mentioned above, all results were gained after averaging over an adequate number of cells, so that the total number of particles simulated was about 3500, even at low filling factors. All data shown refer to room temperature (300 K).

In Fig. 6 we compare the measured intensity profile $I(\boldsymbol{h})$ of sample EMG 909 at zero magnetic field with a simulated

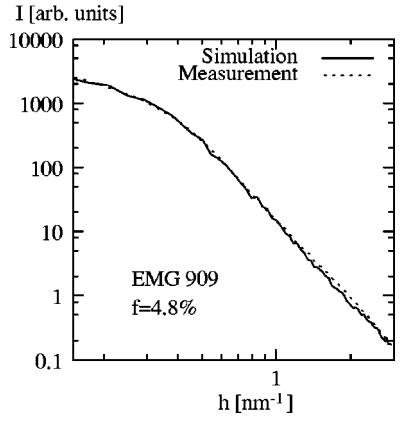

FIG. 6. Double logarithmic plot of measured and simulated scattered intensities vs scattering vector for sample EMG 909 at $B=0$ ($f=2.4\%$). Apart from a scaling (multiplication with a constant) of the simulated intensities no other data processing (e.g., fitting) has been undertaken.

one. At high scattering vectors $h\overline{R}\gg 1$ the scattered intensity is governed by single-particle scattering, a process that depends on shape and orientation of particles [the first term in Eq. (12)]. At smaller scattering vectors also multiple scattering contributes to $I(\boldsymbol{h})$, reflecting the spatial arrangement of particles. The simulated curve is in good agreement with the measured one over the whole range of scattering vectors. For higher particle concentrations (samples EMG 905 and 901a; not shown) the agreement is less good at $h<0.4$ nm^{-1}, i.e., in the range $h\overline{R}<2$ where interparticle interference effects become important. Here the simulated curves yield intensities which are higher than the experimental ones by a factor of approximately 1.5, indicating a deviation between real and simulated particle configuration, at least in dense systems. Probably the simulation underestimates the formation of clusters. This may be caused by the choice of a too low value for A_H, which leads to underestimation of the van der Waals forces. Another explanation would be the simplifications of our model, especially regarding cutting off the large volumes' tail of the particle-size distribution. These bigger particles possess high dipole moments and are responsible for strong dipole-dipole interactions, even in the absence of a magnetic field.

Next, we compare measurements and simulations for a nonzero magnetic field, choosing the saturation value of $B_s=0.3$ T. Since we have used an experimentally determined effective axis ratio in the calculation of the scattering curves, the simulated data will fit the measured ones in the range

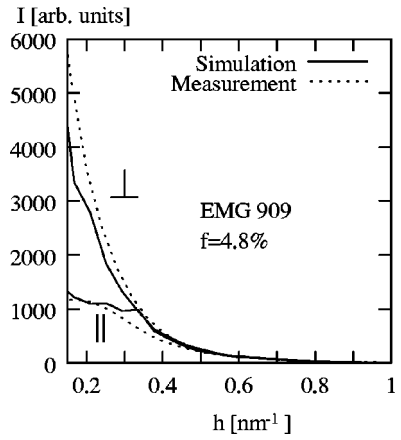

FIG. 7. Simulated and measured scattering intensity parallel and perpendicular to a magnetic field with B=0.3 T for sample EMG909.

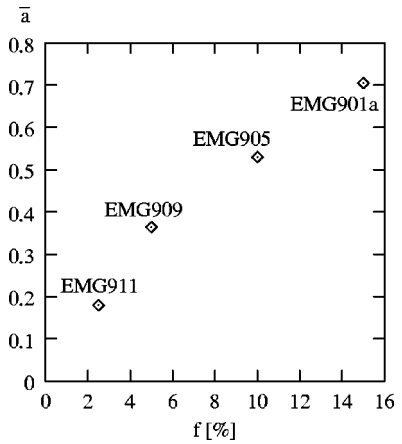

FIG. 8. Total fraction of clustered particles $\bar{\alpha} = V_{clusters}/V_{particles}$ vs volume filling factor (particle concentration) for various samples at magnetic saturation induction $B = 0.3$ T.

where single-particle scattering dominates ($h > 1$ nm). But an independent comparison of measurement and simulation is possible for $h < 1$ nm^{-1}, where the SAXS data reflect cluster formation. Figure 7 shows measurement and simulation results for sample EMG 909. We display scattered intensities for scattering vectors $\boldsymbol{h}$ parallel and perpendicular to the magnetic field, $I_{\parallel}(h)$ and $I_{\perp}(h)$ (for details see Ref. 31). For both directions the simulated scattering intensity shows qualitatively the same dependency on the scattering vector as the experimentally measured one. Again, some quantitative deviations are observed at low scattering vectors, especially for the perpendicular component $I_{\perp}$. Once again, we attribute this to the fact that the simulation underestimates the formation of agglomerates. Nevertheless, the overall agreement is quite satisfactory, allowing us to consider the model presented here as an approximation of real ferrofluid samples. We thus expect that particle arrangements generated by our Monte Carlo simulations reflect the general features of the microstructure, i.e., they should enable us to study the effect of magnetic-field strength on the agglomeration process, especially on size, composition, and form of clusters.

VI. STATISTICAL ANALYSIS OF CLUSTERS: SIZE, COMPOSITION, AND SHAPE

Macroscopic material properties of heterogeneous materials, as they are measured in experiments, reflect the time-averaged microstructure. In our case this is the field-dependent spatial distribution (and orientation) of particles and especially the average number, size, and form of clusters. The latter information can be extracted from Monte Carlo snapshots (equilibrium configurations like the ones in Figs. 4 and 5). With increasing filling factor it becomes more and more difficult to analyze and to distinguish different clusters in such 3D plots. Therefore, we proceed with a statistic evaluation of clusters using the criterion of Eq. (6) (see Fig. 2). In the following, we shall evaluate the size distribution of clusters, their composition (inner-cluster polydispersity) as well as their formation that reflects in a field-dependent shape anisometry.

A. Total agglomerated volume and size distribution of clusters

At first, we calculate the total fraction of clustered particles $\bar{\alpha} = V_{clusters}/V_{particles}$, i.e., the ratio of agglomerated particle volume to the volume of all particles. The values are displayed in Fig. 8. The higher the particle concentration (volume filling factor f) the higher the $\bar{\alpha}$. There is a small field dependence that we shall discuss later (see below, Fig. 13, and Sec. VI C). Here we just want to state that in our samples 20%–80% of the particle mass is found to be in clusters.

The number of particles in these clusters can vary, as the MC snapshots in Figs. 4 and 5 already show. Analytical size distributions have been calculated only for rigid chainlike clusters consisting of equally sized particles, i.e., either for monodisperse systems[8] or for bidisperse systems, in which solely the fraction of large particles is allowed to form clusters[9] (an assumption that is not fulfilled in our polydisperse system; see the Introduction and the following section). Therefore, we now evaluate the probability $p(s)$ that a particle belongs to a cluster of s particles [$s = 1,2,\ldots$ and $\Sigma_s p(s) = 1$]. This is the number of particles that are found in s-particle clusters divided by the total number of particles. The case $s = 1$ corresponds to single particles. Note that for equally sized spheres the definition of $p(s)$ would correspond to that of a volume-weighted cluster-size distribution. But in our polydisperse ferrofluid this is not exact, since the mean particle volume in a cluster slightly depends on s (see the following section). The probability $p(s)$ is displayed in Fig. 9(a) for the respective EMG samples. With increasing particle concentration and thus agglomeration grade the fraction of large clusters increases. In the most concentrated ferrofluid ($f = 15\%$) there exist clusters with more than 100 particles. Nevertheless, $p(s)$ decays with a rate much faster than $1/s$ and the majority of clusters consists of a few particles (dimers, trimers, . . .). This is comparable to what most theoretical models and simulations predict for monodisperse or bidisperse systems at room temperature and zero field, i.e., a mean number of 1–3 particles per cluster.[8,9,20,32,38] Lower-

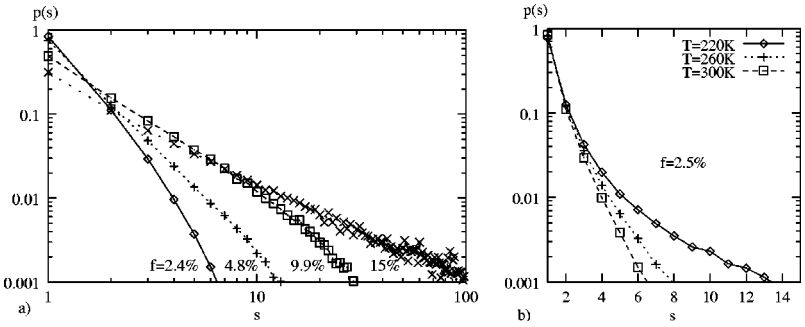

FIG. 9. (a) The probability that a particle belongs to a cluster of s particles for $B=0.3$ T. Note that $s=1$ corresponds to single particles. The higher the particle concentration (volume filling factor f), the higher the fraction of big particles. (b) $p(s)$ for $f=2.5\%$ and $B=0.3$ T at different temperatures. The lower the temperature, the higher the fraction of big clusters.

ing the temperature and thus the thermal energy of particles leads to a higher stability of clusters, so that bigger structures can form [see Fig. 9(b)].

B. Cluster composition: Polydispersity of clustered particles and mean particle size

In this paragraph we focus on the question to what extent particles of different sizes contribute to clusters. We consider a total number of N particles, $N=\int n(R)dR$, a fraction $N_C=\int n_c(R)dR$ of which forms clusters. Here the number-weighted size distribution $n(R)$ denotes the number of particles of radius R. A fraction $n_C(R)$ is clustered, i.e., has at least one neighbor at a center-to-center distance smaller than $r_{ij}^{cluster}$ [see Eq. (6)]. Now let us define an agglomeration probability function,

$$a(R)=\frac{n_c(R)}{n(R)}, \tag{13}$$

indicating the fraction of particles of size R belonging to clusters $(0\leqslant a(R)\leqslant 1)$. Figure 10(a) shows $a(R)$ for the simulated systems at $B=0.3$ T. There is only a small field dependence that we shall discuss later [see Fig. 10(b)]. The clustering probability becomes higher with increasing particle size and increasing particle concentration. In order to control to what extent this effect is due to the higher dipole moment of the larger particles, we also conducted simulations on control systems having the same concentration and particle-size distribution but with no interparticle interactions [Fig. 10(b), lower curve]. The comparison shows that there is a mere geometrical effect due to the random positioning of the particles in space: big particles have a larger surface and thus a higher probability that another particle will find itself in their vicinity. Summarizing, larger particles have a stronger tendency to form agglomerates, both due to their high dipole moment and their large surface. Returning to the samples with interactions, Fig. 10(a) shows that already at a particle volume concentration of 4.8% and at $B=0.3$ T, 75% of the particles with radii of 10 nm belong to clusters, at zero field even 90% (not shown). But we have to keep in mind that there are only a few particles of this size that make up solely a small portion of the clustered mass. Smaller particles, which are more numerous and represent a higher volume fraction (see Fig. 1), have also a not negligible probability to agglomerate. For example, at $f=4.8\%$ about 25% of particles with a radius equal to the mean radius $\overline{R}=4.5$ nm belong to clusters, at $f=15\%$ even 60% (values independent of magnetic induction B). Qualitatively, we can confirm the picture given in the theoretical model of Ref. 38 describing a bidisperse system: most of the large and a considerable fraction of small particles is aggregated.

Next, we are interested in determining a mean particle size of clustered particles. But not all clusters necessarily exhibit the same composition: the higher the number of particles in a cluster, s, the higher the average volume of these particles, $\overline{V_p}(s)$ (see Fig. 11). This behavior reflects the aforementioned fact that big particles have a higher agglomeration probability. As a consequence, clusters with many particles preferably form around big particles. Correspondingly, single particles $(s=1)$ have the smallest average size. However, the variation is rather small, i.e., $\overline{V_p}(s)$ is of the

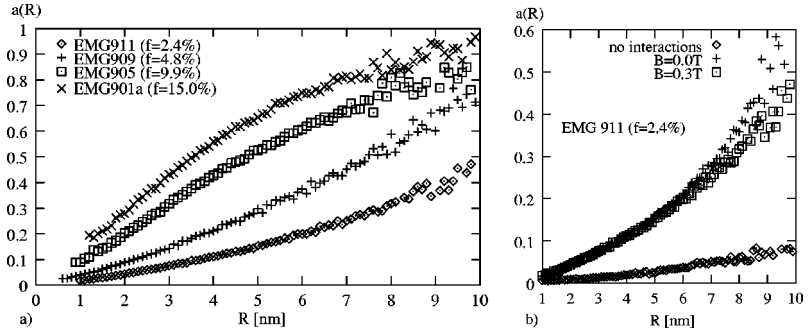

FIG. 10. (a) The fraction of particles belonging to a cluster [agglomeration probability $a(R)$; see Eq. (13)] as a function of particle radius R for different samples at $B=0.3$ T. The higher the particle concentration, the higher the degree of agglomeration. (b) $a(R)$ for the lowest particle concentration at $B=0$ and $B=0.3$ T (upper curves). The lower curve refers to the simulation of a control system with the same concentration and distribution of particle sizes, but without any interactions (random spatial distribution of particles; see text).

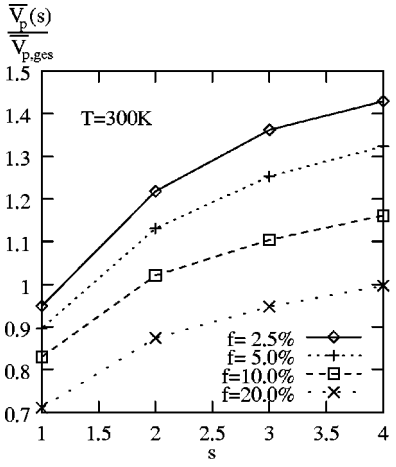

FIG. 11. Ratio of average particle volume in a cluster, $\overline{V_p}(s)$, over the overall average particle volume, $\overline{V_{p,tot}}$, vs the number of particles in a cluster, s. In order to show more clearly the influence of cluster size, we display curves corresponding to systems with different concentrations but having the same size distribution (that of sample EMG 911). $s=1$ corresponds to single particles.

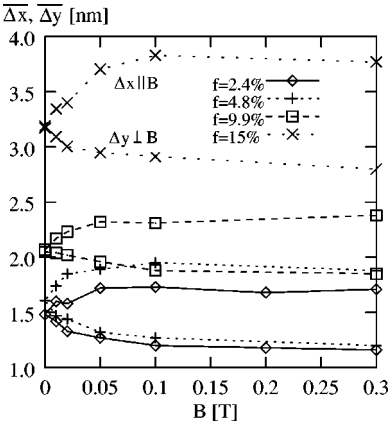

FIG. 12. Cluster elongations parallel ($\overline{\Delta x}$, upper curves) and perpendicular ($\overline{\Delta y}$, lower curves) to a magnetic induction $B=B_x$. The displayed average values are number weighted and increase with increasing particle concentration of the samples. The range of magnetic induction, $B=0-0.3$ T, corresponds to a range of Langevin parameters $\mu_{av}H/k_BT=0-12.4$, where μ_{av} is the dipole moment of a particle with average radius 5 nm (see Sec. III A).

order of the mean particle volume of all particles in the ferrofluid, $\overline{V_{p,tot}}$. For the most part of the clustered mass (compare with Fig. 9 for $s\geqslant 2$) in all samples $0.85\times\overline{V_{p,tot}} \leqslant \overline{V_p}(s) \leqslant 1.45\times\overline{V_{p,tot}}$ holds. This corresponds to mean radii in s-particle clusters of $\overline{R(s)}\simeq 0.95\times\overline{R}-1.1\times\overline{R}$. In other words, the volume-weighted mean particle radius in clusters roughly equals the mean radius of all particles, $\overline{R}\simeq 4-5$ nm (see Fig. 1). Thus, our simulations confirm what we have previously measured in 2D-SAXS experiments:[31] although the agglomeration probability increases with increasing particle size, a polydisperse ferrofluid cannot be divided in two subsystems of small single particles and large agglomerating particles. Single particles ($s=1$) are, on an average, rather small, but this does not imply at all that only big particles form clusters. On the contrary, there is a sufficiently large portion of small particles taking part in cluster formation. Therefore, the polydispersity of particles reflects in the composition of clusters.

C. Field-dependent cluster formation and shape anisometry of clusters

Since we want to characterize the average shape of clusters in a simple way, we evaluate their elongation parallel (Δx) and perpendicular to the field axis (Δy). In order to take the irregularity of cluster forms into account, contributions of clustered particles are volume-weighted. In field direction, this reads for a given cluster as

$$\Delta x = \frac{\sum_{j=1}^{s} |x_j - x_c| V_j}{\sum_{j=1}^{s} V_j}, \tag{14}$$

where $s\geqslant 2$ is the number of particles belonging to the cluster, x_j and V_j denote position and volume of particle j, and $x_c=\Sigma_{j=1}^{s} x_j V_j / \Sigma_{j=1}^{s} V_j$ is the coordinate of the cluster's center of gravity along the field axis $\hat{\boldsymbol{x}}$. Δy is calculated correspondingly. These volume-weighted elongations are not to be confused with the absolute extension of a cluster. For example, taking a linear chain consisting of a big particle of 20 nm diameter with an 8 nm particle at each side we obtain a chain length of $l=36$ nm but $\Delta x\simeq 1.6$ nm. Note that the relation between l and Δx strongly depends on the degree of polydispersity. Only for linear chains of monodisperse particles there is a simple relation allowing one to determine the chain length: $l\simeq 4\Delta x$ holds in a good approximation for $s>1$ ($l=4.5\Delta x$ at $s=3$). But as already mentioned we do not want to restrict the data evaluation to linear chains and thus we use the above volume-weighted extensions. For the cluster sizes we refer to Fig. 9.

In Fig. 12 we display number-weighted average values $\overline{\Delta x}$ and $\overline{\Delta y}$ for our samples. The higher the particle concentration the bigger the clusters. At zero field $\overline{\Delta x}=\overline{\Delta y}$ holds, i.e., single clusters, which are surely not perfectly spherical (isometric), have a random orientation. With increasing magnetic field $\overline{\Delta x}$ increases while $\overline{\Delta y}$ decreases. Partly this is due to an alignment of clusters in field direction. In addition, there is a rearrangement of particle positions in clusters. The latter process reflects in the field dependence of the clustered mass fraction $\overline{\alpha}$ (see Fig. 13): increasing the magnetic induction up to its saturation value leads to a 10% decrease of the agglomerated mass [a comparison with Fig. 10(b) shows that especially larger particles with radii $R>5$ nm contribute to this field dependence]. At first glance this seems surprising, but it is just a consequence of the anisotropic character of dipolar interactions between particles whose magnetic moments are aligned: while the attraction is reinforced when

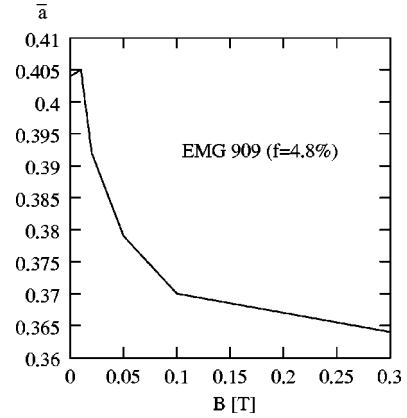

FIG. 13. Total fraction of clustered particles vs magnetic induction for sample EMG 909.

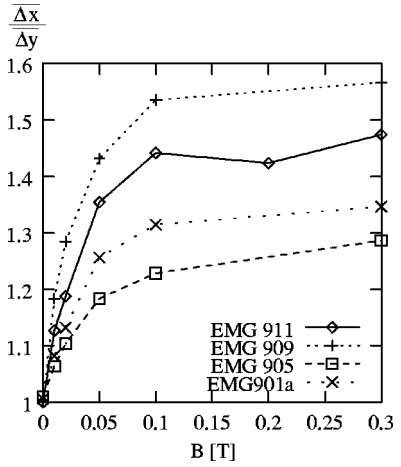

FIG. 14. Average shape anisometry of clusters as a function of magnetic induction.

nose-to-tail-like chains form, lateral particles are repelled, so that the perpendicular cluster extension Δy as well as the volume fraction of agglomerated particles decrease (Figs. 12 and 13). The cluster extension in field direction increases, both due to the above rearrangement of particles and due to field-dependent cluster orientation (Fig. 12).

The field dependence of shape anisometry, i.e., the ratio $\overline{\Delta x}/\overline{\Delta y}$ is displayed in Fig. 14. It follows qualitatively the Langevin function describing the magnetization of paramagnetic systems. With increasing magnetic field agglomerates become elongated with their longer dimension in the direction of the field. The changes in the cluster shape reach saturation at magnetic fields of the order of 0.3 T, which is also the saturation field for the magnetization of the studied ferrofluids.[31] Simulations for samples with identical size distribution reveal that thermal disorder (increase of temperature) or a higher particle concentration (increase of cluster size) leads to a decrease of shape anisometry (not shown).

The above field-dependent anisometry values $\overline{\Delta x}/\overline{\Delta y}(B)$ have been obtained by averaging over clusters of all sizes (see Fig. 9). They reflect both geometrical form and orientation. The knowledge of these parameters is of practical relevance, especially in nonequilibrium flow situations: the field-dependent viscosity of ferrofluids, for example, depends on the polydispersity of clusters[8,9] and is even an explicit function of the cluster shape.[10,11] Nonspherical agglomerates are often described in terms of axis ratios. Depending on the fluids studied, the measured properties, and the theoretical models/approximations used for the data evaluation, values in the range 1–2 can be found in the literature.[10,28,32,39,53]

VII. CONCLUSIONS

We have presented Monte Carlo simulations of ferrofluids using parameters based on existing ferrofluid samples and taking magnetic dipole-dipole, van der Waals, and steric interactions as well as the polydispersity of the samples into account. The obtained equilibrium configurations were found consistent with experimental 2D-SAXS data, a fact showing that the simulations allow us to gain information on the microstructure of real polydisperse systems. Even in the absence of a magnetic field a large number of the particles forms clusters. These consist mostly of a small number of particles, but in the most concentrated systems clusters of up to 100 particles exist. Although the majority of single particles are of small radii and the agglomeration probability increases with increasing particle size, there is a sufficiently large fraction of small particles taking part in cluster formation. As a consequence, the mean radius of clustered particles is approximately equal to the overall mean particle radius $\bar{R}$. There is no division in two subsystems of small single particles and large agglomerating particles. The change of microstructure in an applied magnetic field is due to both the orientation of clusters and to the increase of their shape anisometry.

ACKNOWLEDGMENTS

The authors are grateful to Professor Günter Nimtz for hosting this work in his laboratory. The project was supported by the European Commission under TMR Marie Curie Grant No. ERBFMBICT982913 (A.S.) and by the DFG under Project No. Ni/49/33-1.

[1] R.E. Rosensweig, *Ferrohydrodynamics* (Cambridge University Press, New York, 1985).
[2] *Ferrofluids, Magnetically Controllable Fluids and their Applications*, edited by S. Odenbach, Lecture Notes in Physics Vol. 594 (Springer-Verlag, Berlin, 2002).
[3] B.Z. Kaplan and D.M. Jacobson, Nature (London) **259**, 654 (1976).
[4] A.J. Mailfert and B. Nahounou, IEEE Trans. Magn. **16**, 254 (1980).
[5] H.W. Davies and J.P. Llewellyn, J. Phys. D **13**, 2327 (1980).
[6] J.J.M. Janssen and J.A.A.J. Perenboom, J. Magn. Magn. Mater. **81**, 14 (1989).
[7] N.A. Yusuf, J. Shobaki, H. Abu-Safia, and I. Abu-Aljarayesh, J. Magn. Magn. Mater. **149**, 373 (1995).

[8] A.Y. Zubarev and L.Y. Iskakova, Phys. Rev. E **61**, 5415 (2000).
[9] A.Y. Zubarev, Zh. Eksp. Teor. Fiz. **120**, 94 (2001) [JETP **93**, 80 (2001)].
[10] P. Ilg and M. Kröger, Phys. Rev. E **66**, 021501 (2002).
[11] M. Kröger, P. Ilg, and S. Hess, J. Phys.: Condens. Matter **15**, S1 403 (2003).
[12] R. Chantrell, A. Bradbury, J. Popplewell, and S.W. Charles, J. Phys. D **13**, L119 (1980).
[13] R. Chantrell, A. Bradbury, J. Popplewell, and S.W. Charles, J. Appl. Phys. **53**, 2742 (1982).
[14] G. Helgesen, A.T. Skjeltorp, P.M. Mors, R. Botet, and R. Jullien, Phys. Rev. Lett. **61**, 1736 (1988).
[15] S. Menear, A. Bradbury, and R. Chantrell, J. Magn. Magn. Mater. **43**, 166 (1984).
[16] D.Q. Wei and G.N. Patey, Phys. Rev. Lett. **68**, 2043 (1992).
[17] J.J. Weis and D. Levesque, Phys. Rev. Lett. **71**, 2729 (1993).
[18] M.J. Stevens and G.S. Grest, Phys. Rev. Lett. **72**, 3686 (1994).
[19] M.J. Stevens and G.S. Grest, Phys. Rev. E **51**, 5962 (1995).
[20] S.W. Davis, W. McCausland, H.C. McGahagan, C.T. Tanaka, and M. Widom, Phys. Rev. E **59**, 2424 (1999).
[21] P.J. Camp and G.N. Patey, Phys. Rev. E **62**, 5403 (2000).
[22] V.V. Murashov, P.J. Camp, and G.N. Patey, J. Chem. Phys. **116**, 6731 (2002).
[23] A.F. Pshenichnikov and V. Mekhonoshin, Eur. Phys. J. E **6**, 399 (2001).
[24] R. van Roij, Phys. Rev. Lett. **76**, 3348 (1996).
[25] M.E. van Leeuwen and B. Smit, Phys. Rev. Lett. **71**, 3991 (1993).
[26] M.J. Stevens and G.S. Grest, Phys. Rev. E **51**, 5976 (1995).
[27] M.J. Blair and G.N. Patey, Phys. Rev. E **57**, 5682 (1998).
[28] M.F. da Silva and A.M.F. Neto, Phys. Rev. E **48**, 4483 (1993).
[29] C.Y. Matuo and A.M.F. Neto, Phys. Rev. E **60**, 1815 (1999).
[30] L.N. Donselaar, P.M. Frederik, P. Bomans, P.A. Buining, B.M. Humbel, and A.P. Philipse, J. Magn. Magn. Mater. **201**, 58 (1999).
[31] T. Kruse, H.-G. Krauthäuser, A. Spanoudaki, and R. Pelster, Phys. Rev. B **67**, 094206 (2003).
[32] K.I. Morozov, Phys. Rev. E **66**, 011704 (2002).
[33] S. Odenbach and H. Störk, J. Magn. Magn. Mater. **183**, 188 (1998).
[34] J.C. Bacri, R. Perzynski, D. Salin, V. Cabuil, and R. Massart, J. Colloid Interface Sci. **132**, 43 (1989).
[35] V. Russier and M. Douzi, J. Colloid Interface Sci. **162**, 356 (1994).
[36] B.J.C. Cabral, J. Chem. Phys. **112**, 4351 (2000).
[37] R.W. Chantrell, G.N. Coverdale, M.E. Hilo, and K. O'Grady, J. Magn. Magn. Mater. **157-158**, 250 (1996).
[38] S. Kantorovich and A.O. Ivanov, J. Magn. Magn. Mater. **252**, 244 (2002).
[39] S. Odenbach and H.W. Müller, Phys. Rev. Lett. **89**, 037202 (2002).
[40] *Dispersion Forces*, edited by J. Mahanty and B.W. Ninham (Academic Press, New York, 1976).
[41] L. Bergström, Adv. Colloid Interface Sci. **70**, 125 (1997).
[42] J.N. Israelachvili, *Intermolecular and Surface Forces* (Academic Press Inc., San Diego, 1985).
[43] D. Levesque and J.J. Weis, Phys. Rev. E **49**, 5131 (1994).
[44] N. Metropolis, A.W. Rosenbluth, M.N. Rosenbluth, A.H. Teller, and E. Teller, J. Chem. Phys. **21**, 1087 (1953).
[45] M.P. Allen and D.J. Tildesley, *Computer Simulations of Liquids* (Clarendon Press, Oxford, 1987).
[46] J.-O. Andersson, C. Djurberg, T. Jonsson, P. Svedlindh, and P. Nordblad, Phys. Rev. B **56**, 13 983 (1997).
[47] J.A. Barker and R.O. Watts, Mol. Phys. **26**, 789 (1973).
[48] J.A. Barker, in *NRCC Workshop Proceedings*, 1980, Vol. 9, pp. 45 and 46.
[49] S.W.D. Leeuw, J.W. Perram, and E.R. Smith, Proc. R. Soc. London, Ser. A **373**, 27 (1980).
[50] H.L. Friedman, Mol. Phys. **29**, 1533 (1975).
[51] J.S. Pedersen, Adv. Colloid Interface Sci. **70**, 171 (1997).
[52] T. Kruse, Ph.D. thesis, Universität zu Köln, Köln, 2000.
[53] A. Grants, A. Irbitis, G. Kronkalns, and M.M. Maiorov, J. Magn. Magn. Mater. **85**, 129 (1990).